Arch. Metall. Mater. **62** (2017), 4, 1969-1981

DOI: 10.1515/amm-2017-0295

Z. EBRAHIMI*#

MODELING OF EUTECTIC FORMATION IN Al-Si ALLOY USING A PHASE-FIELD METHOD

We have utilized a phase-field model to investigate the evolution of eutectic silicon in Al-Si alloy. The interfacial fluctuations are included into a phase-field model of two-phase solidification, as stochastic noise terms and their dominant role in eutectic silicon formation is discussed. We have observed that silicon spherical particles nucleate on the foundation of primary aluminum phase and their nucleation continues on concentric rings, through the Al matrix. The nucleation of silicon particles is attributed to the inclusion of fluctuations into the phase-field equations. The simulation results have shown needle-like, fish-bone like and flakes of silicon phase by adjusting the noise coefficients to larger values. Moreover, the role of primary Al phase on nucleation of silicon particles in Al-Si alloy is elaborated. We have found that the addition of fluctuations plays the role of modifiers in our simulations and is essential for phase-field modeling of eutectic growth in Al-Si system. The simulated finger-like Al phases and spherical Si particles are very similar to those of experimental eutectic growth in modified Al-Si alloy.

Keywords: Phase-field model; Al-Si alloy ; Eutectic growth; Fluctuations

1. Introduction

The eutectic Al-Si alloy is one of the most widely used aluminum-based alloys and has attracted commercial attention, specially in automotive and aerospace industries. Many experimental studies are performed to investigate the nature of eutectic silicon growth, in Al-Si alloy during solidification and refining processes. The precipitation of silicon in Al-Si alloy has also been studied experimentally by many researches, including solidification refining from Al-Si melt [1], eutectic nucleation [2], irregular eutectic Al-Si [3] and hypo-eutectic Al-Si alloys [4]. The formation and chemical modification of the Al-Si eutectic is reviewed in Ref. [5], in which the mechanisms and crystallography of the Al-Si eutectic reaction are presented.

It has been established that the Al-Si eutectic can exhibit either an unmodified or a modified morphology. Silicon in unmodified Al-Si eutectics has the flake-like microstructure [6]. However, in the microstructure of a chemically modified alloy, the silicon particles appear as isolated spherical crystals. The eutectic in modified alloys tends to grow from the surface of a casting towards the center, while that in unmodified alloys tends to grow randomly within the melt [7]. For the commercial Al-Si alloys, microstructural modifications have been made by adding modifiers, such as strontium or sodium, to the melt. Modifier additions, affects the nucleation of silicon in Al-Si alloys and plays a dominant role in the modification of the Al-Si eutectic [6]. Recent experiments by Bian et al. [8] give a more compelling evidence that the morphology of the Al-Si eutectic is decided during its nucleation in the liquid. Makhlouf and Guthy [5] have also stated that modifier additions alter the solid-liquid interface energies during solidification, and thus affect the Al-Si eutectic nucleation kinetics.

Typical eutectic structures of binary alloys form by the simultaneous growth of two phases from the liquid and exhibit a variety of microstructures. The two morphologies that are most frequently observed in eutectic composites are lamellae of the two phases, and rods (fibrous morphology) of one phase surrounded by a matrix of the other phase [9]. Lamellar eutectic patterns in bulk-sample solidification have been studied both in experiments and simulations [10,11]. One of the most significant theoretical studies in eutectic growth is the work of Jackson and Hunt [12]. They have found that, for a given interface velocity, stable growth occurs at minimum interface undercooling. Rod-like eutectics tend to form when the volume fractions of the two phases are strongly different. Akamatsu and Plapp have reviewed the various phenomena that influence the dynamics of two-phase pattern formation and morphological transformations of lamellar and rod eutectics [13]. They have stated that the eutectic patterns can be dramatically influenced by crystallography. The influence of interphase boundary anisotropy on lamellar eutectic growth is established recently [14].

In general, there is a contribution to the free-energy of solid-liquid interface emerging from the fluctuations in the interface region, which brings about the natural nucleation phe-

* PAYAME NOOR UNIVERSITY, DEPARTMENT OF MECHANICAL ENGINEERING, PO BOX 19395-3697 TEHRAN, IRAN

Corresponding author: z.ebrahimi@pnu.ac.ir

nomena [16,15]. The proper treatment of nucleation process in the phase-field model, requires the introduction of stochastical noise terms into the governing equations [17]. The noise terms allow heterogeneous nucleation leading a system from metastable state to stable state. A phase-field model of the grain nucleation during solidification, in which the fluctuations are incorporated into the phase-field equation by additional source terms is given in Ref. [18].

The phase-field method is used intensively in modeling of microstructure evolution in phase transformation of pure materials, alloys and other material systems. It is a genuine representation of the original free-boundary problem in sharp-interface limit as the interface thickness tends to zero. In the past decade, many applications of this method have been reported [19]. Phase-field method is a suitable tool to model the formation of complex solidification interfaces and prediction of microstructure in many material systems like coherent solid-state phase transitions [20,21], multiphase growth [22,23], competitive growth of dendrites [24 25] and dendritic solidification in binary alloys [26,27]. A review on the application of the phase-field method in phase transitions is given in Ref. [28].

One of the first applications of the phase-field approach in alloys solidification has been introduced by Wheeler and colleagues [29]. The phase-field model has been successfully applied to study the coherent precipitation of ordered intermetallics from a disordered fcc solid solution in Ni-base alloys [30], in which the formulation of the free energy is based on the concentration wave representation of the ordered state. In a different way, Folch and Plapp have developed a phase-field model for eutectic and peritectic solidification, in which a smooth free energy functional is used to connect any two phases [11]. The work of Folch and Plapp has been further extended to include anisotropic elasticity and mis-orientations in eutectic growth [17,31], in which the free energy of the system consists of a chemical free energy and an elastic free energy.

In this paper, we investigate the nucleation and growth of eutectic silicon in Al-Si alloy by phase-field simulations. First, we have included interfacial fluctuations, as stochastic noises, in the Folch-Plapp (FP) phase-field model to simulate eutectic formation in Al-Si alloy. We have shown that these fluctuations play the role of modifier additions in the Al-Si system. We have performed phase-field simulations for two values of β-Si composition, to elaborate its effect on the size of silicon particles and the eutectic spacing. The magnitudes of fluctuations in eutectic growth, and their effects on silicon morphology are also studied. Moreover, we have studied the role of primary α-Al in nucleation of silicon particles in Al-Si alloy. We have observed finger-like α-Al phases, which provided a nucleation site for β-Si particles, in our simulations. The formation of these α-Al fingers and spherical silicon particles have been reported in experiments of eutectic reaction in modified Al-Si alloy. The good agreement, which is obtained between our simulation results and experimental observations, elaborates the role of fluctuations in modeling of eutectic growth. The presented phase-field model can be used to predict the microstructure of eutectic silicon in Al-Si alloy, which are costly and difficult to perform experimentally. We have represented the related phase-field equations in the first part of this paper. The numerical parameters are discussed later and the simulations results are illustrated.

2. Phase-field model

In the concept of the phase-field method, a diffuse interface with a limited thickness is assumed between two different phases. The interfacial conditions are avoided by introducing a set of smooth variables, the so-called phase-field variables, which characterize time and spacial evolutions of bulk phases in the underlying system. The phase-field variables represent bulk phases and interfaces in the material system, and usually take the value of 1 in the corresponding phase and zero outside of it. By using the differential equations of the phase-field variables, which are consistent with the material thermodynamics in phase transformations, tracking of the interfaces and applying the moving boundary conditions, which are often very complex, can be avoided [19].

In a binary eutectic alloy, two distinct solid phases, α and β, coexist with the liquid phase at the eutectic temperature T_E. If both solid phases have isotropic and non-faceted solid-liquid interfaces, the theoretical description of their growth includes bulk diffusion in the liquid phase, mass conservation at the moving interfaces, which is known as Stefan condition, local equilibrium at interfaces, which is given by Gibbs-Thomson equation, and local equilibrium at trijunction points. The corresponding free-boundary problem can be found in Ref. [32].

To construct the evolution equations for phase-field variables, we interpret the phase-field variables as order parameters. Their time evolution is considered to be a relaxation towards the minimum of a free-energy functional, in the spirit of the time-dependent Ginzburg-Landau models for the out-of-equilibrium thermodynamics of phase transitions. In this paper we use the FP model for two phase solidification and include the interfacial fluctuations as noise terms in the phase-field equations. We should note that the FP model has not been linked to explicit thermodynamic formulation. It has used a free energy functional, which is capable of simulating the the free boundary problem efficiently [11]. In that model the dynamics of the solid-liquid interfaces were accurately simulated and were independent of the interface thickness for sufficiently thin interfaces, as predicted by the asymptotic analysis.

The starting point for any asymptotic analysis is the equilibrium front solution that connects two different bulk phases. For a binary alloy, there are two or more coupled nonlinear partial differential equations in terms of the composition and one or more phase fields. In the thin-interface limit, in which W is small but finite, we choose the coupling terms such that they vanish in equilibrium, as in available Refs. [11, 22].

We denote each phase-field variable by ϕ_i, which is unity in the corresponding i-th single phase region and zero outside that phase, i.e. $\phi_i \in [0,1]$, and varies smoothly between these two

values. $\phi_i = 1$ then represents the domain where phase i exists, $\phi_i = 0$ where it absent and $0 < \phi_i < 1$ its bounding interfaces. The phase-field variables should satisfy $\sum_i \phi_i = 1$. In eutectic growth, the index i represents two solid phases (α, β) and one liquid phase (L).

Traditional phase-field models are connected to thermodynamics by a phenomenological free energy functional, written in terms of the phase-field and other fields, such as temperature and concentrations. Through a dissipative minimization of this free energy, the dynamics of one or more order parameter, as well as those of heat or mass transfer are governed by set of non-linear partial differential equations.

In phase-field models of eutectic growth in binary alloys, the free energy density is a functional of three phase-filed variables $\vec{\phi} = (\phi_\alpha, \phi_\beta, \phi_L)$ a concentration c and a temperature T. The total free energy of the material system is described by the volume integral of the free energy density, as introduced in Ref. [11],

$$F = \int_V f\left(\vec{\phi}, c, T\right) dV \tag{1}$$

where the bulk free energy density, $f(\vec{\phi}, c, T)$, is given by

$$f\left(\vec{\phi}, c, T\right) = \frac{\varepsilon_\phi^2 \left|\vec{\nabla}\vec{\phi}\right|^2}{2} + Hf_p\left(\phi_i\right) + Xf_{ch}\left(\phi_i, c, T\right) \tag{2}$$

where $\varepsilon_\phi = \sqrt{HW}$ is a constant that sets the interface energy and has the unit of energy per unit length, $[\mathrm{J/m^3}]^{1/2}$ and the gradient term on rhs of Eq. (2) is the kinetic part of the free energy density. The constant W sets the length scale of the interfaces. The constants H and X have the dimension of energy per unit volume $[\mathrm{J/m^3}]$. X is the dimensional prefactor of the concentration-dependent terms and hence sets the magnitude of the thermodynamic driving forces, which is a macroscopic and physically measurable quantity. In contrast, ε_φ and H can be adjusted in order to achieve a desired surface tension and interface thickness.

The dimensionless functions f_p and f_{ch} must have three local minima to account for three possible phases, which are the solid phases, α and β, and the liquid phase, L. The function f_{ch} is the double well potential, which has three minima for the phase-field variables of the system. The simplest choice for f_p, which is usually used in the phase-filed models, is

$$f_p\left(\phi_i\right) = \sum_i \phi_i^2 \left(1 - \phi_i\right)^2 \quad \text{for} \quad i = \alpha, \beta, L \tag{3}$$

Structural transformations in alloys involves the mass transport. The transformation that we consider here, is the eutectic growth of α-Al and β-Si phases in Al-Si alloy. Two concentration fields are defined in this case, one for the Al phase, c_α, and another for the Si phase, c_β. $c = (C - C_E)/\Delta C$ is the dimensionless concentration, where C_E is the eutectic composition, $\Delta C = C_\beta - C_\alpha$ and C_α and C_β are the compositions of α and β phases at eutectic temperature, respectively.

The function f_{ch} is the chemical free energy density, which determines the phase-diagram of the alloy and is defined as

$$f_{ch}\left(\phi_i, c, T\right) = \frac{1}{2}\left(c - \sum_i c_i g_i\left(\phi_i\right)\right)^2 + \sum_i B_i(T) g_i\left(\phi_i\right) \tag{4}$$

where c_i is the concentration of the phase i in equilibrium with another phase and B_i is the free energy density of phase i.

The relative stability of the phases depends on the concentration values. This requires addition of a function to the free energy density that tilts the double well by an amount proportional to the local driving forces [11]. We construct a function g_i that tilts the double well and besides keeps the minima of the free energy at fixed values $\phi_i = 0, 1$ independent of the value of c. In other words, $g_i(\vec{\phi})$ should be a monotonic function satisfying $g_i(\phi_i = 0) = 0$ and $g_i(\phi_i = 1) = 1$. We construct the tilting function g_i, analogous to available models of eutectic solidification [11,19], as follows

$$g_i\left(\vec{\phi}\right) = \frac{\phi_i^2}{4}\left(\begin{array}{l} 15\left(1 - \phi_i\right)\left[1 + \phi_i - \left(\phi_k - \phi_j\right)^2\right] + \\ + \phi_i\left(9\phi_i^2\right) \end{array}\right) \tag{5}$$

where the index i, j and k represent possible phases in the system.

We define the chemical potential μ as the variation of F with respect to the concentration c,

$$\mu = \frac{1}{X}\frac{\delta F}{\delta c} = c - \sum_i c_i g_i\left(\phi_i\right) \quad \text{for} \quad i = \alpha, \beta \tag{6}$$

The concentration field c evolves according to the mass conservation equation,

$$\frac{\partial c}{\partial t} = \vec{\nabla} \cdot \left(M\left(\vec{\phi}\right)\vec{\nabla}\frac{\delta F}{\delta c}\right) \tag{7}$$

where $M(\vec{\phi})$ is the chemical mobility. Substituting the chemical potential given by Eq. (6) in Eq. (7), the mass conservation equation becomes,

$$\frac{\partial \mu}{\partial t} = \vec{\nabla} \cdot \left(D\left(\vec{\phi}\right)\vec{\nabla}\mu\right) - \sum_i c_i \frac{\partial g_i\left(\vec{\phi}\right)}{\partial t} \tag{8}$$

where $D(\vec{\phi}) = XM(\vec{\phi})$ is a phase dependent diffusivity. In our model, we consider the diffusivity as $D(\vec{\phi}) = D\phi_L$, where D is the diffusion coefficient of the liquid phase.

The temporal evolution of the two non-conserved phase-field variables, ϕ_α, ϕ_β, gives the location of interface between the solid and liquid phases and is a relaxation toward the minimum of the free-energy functional F,

$$\tau\left(\vec{\phi}\right)\frac{\partial \phi_i}{\partial t} = -\frac{1}{H}\frac{\delta F}{\delta \phi_i}\Big|_{\phi_\alpha + \phi_\beta + \phi_L = 1} + \eta_i \tag{9}$$

for $i = \alpha, \beta$. $\tau(\vec{\phi})$ is a relaxation time and controls the time of attachment of atoms to solid interfaces. η_i is the stochastic noise term in the eutectic system, which should be included in the phase-field equation to simulate fluctuations at the solid-liquid interface. The noise terms allow heterogeneous nucleation leading a system from metastable state to stable state. To model the

interfacial fluctuations, we introduce η_i as an additional term into the phase-filed equations,

$$\eta_i = R_i(t)N_i\left(1-\phi_i\right) + \\ + R_L(t)N_L\phi_L\left(1-\phi_L\right)\left(i=\alpha,\beta\right) \quad (10)$$

where R_i and R_L are random numbers between zero and one, N_i and N_L are the magnitude of the fluctuations and ϕ_L is the phase-field variable for the liquid phase. Since we have the constraint $\phi_\alpha + \phi_\beta + \phi_L = 1$ in our phase-field model, we can consider the equation of motion (Eq. 9) for the solid phases only. The evolution of the liquid phase is then computed as, $\phi_L = 1 - \phi_\alpha - \phi_\beta$.

The derivative $\delta F/\delta\phi_i|_{\phi_\alpha+\phi_\beta+\phi_L=1}$ in Eq. (9) can be evaluated by the method of Lagrange multipliers analogous to Ref. [11]. Using this and replacing the components of the free energy density, f_p (Eq. 3) and f_{ch} (Eq. 4) in Eq. (9) we obtain the evolution of solid phases as,

$$\tau\left(\vec{\phi}\right)\frac{\partial\phi_i}{\partial t} = W^2\nabla^2\phi_i + \frac{2}{3}\left[\begin{array}{l}-2\phi_i\left(1-\phi_i\right)\left(1-2\phi_i\right)+\\ +\sum_{j\neq i}\phi_i\left(1-\phi_i\right)\left(1-2\phi_i\right)\end{array}\right] - \\ -\frac{\lambda_c}{2}\frac{\partial g_j}{\partial\phi_i}\left(\mu c_j - B_j\right) + \eta_i, \quad i=\alpha,\beta \quad (11)$$

where $W = \varepsilon_\phi/\sqrt{H}$ is the thickness of the interface between the solid phase. $\lambda_c = X/H$ is a coupling constant that connects the phase-field model to the material parameters and the phase-diagram of the alloy. The coupling constant, λ_c, is determined in the thin-interface limit, such that the couplings vanish in equilibrium. The Gibbs-Thomson boundary condition is satisfied by the following coupling constant and relaxation times. See Ref. [11] for more details.

$$\lambda_c = \frac{W}{\bar{d}}\frac{a_1}{2}\left(\frac{1}{|c_\alpha|}+\frac{1}{|c_\beta|}\right) \quad (12)$$

The relaxation time τ_i is obtained for arbitrary kinetics,

$$\tau_i = \lambda_c W|c_i|\left(\frac{\kappa_i}{a_1}a_2\frac{|c_i|W}{D}\right), \quad i=\alpha,\beta \quad (13)$$

where $a_1 = \sqrt{2}/3$ and $a_2 = 0.7464$ are numerical constants. κ_i is the kinetic coefficient of the i-th phase. The parameter λ_c controls the ratio of the interface thickness, W, to the average capillary length, $\bar{d}$. As stated before, the phase-field model is independent of W for sufficiently thin interfaces. The interface thickness W should be larger than the average capillary length, $\bar{d}$, to make the phase-field simulations feasible [19]. Therefore, we choose $W/\bar{d}$ as the resolution for our model in a way that fulfills the above requirement.

The initial conditions are substituted into the phase-field evolution equations (Eq. 11). The phase-filed equations are solved together with the diffusion equation (Eq. 8), and the phase-filed variables ϕ_α, ϕ_β and the concentration c are evaluated at each time step.

3. Model parameters

The Al-Si system is a simple binary eutectic with limited solubility of aluminum in silicon. The solubility of silicon in aluminum reaches a maximum 1.5 at.% at the eutectic temperature. There is only one invariant reaction in this diagram, namely the eutectic reaction. L is the liquid phase, α is predominantly aluminum, and β is predominantly silicon. It is now widely accepted that the eutectic reaction takes place at 577C° and at a silicon level of 12.6%. Fig. 1 represents a schematic of Al-Si phase diagram, according to Murray and McAlister work [33].

Cao et al. have assessed the impurity diffusion coefficients of Si in fcc-A1 Al using DICTRA software package and have compared the calculated coefficients with the experimental data from the literature, satisfactorily [34]. We use the value of $D = 0.5 \times 10^{-12}$ m^2/s in our simulations, according to their study. In our phase-field model, the temperature is kept constant, when isolated nuclei of α-β solid phases are growing into the liquid. We use a constant undercooling in our simulations. The solidification and eutectic temperatures are 540C° and 577C°, respectively.

The model parameters used in the phase-field simulations are listed in Table 1, where m_α and m_β are the liquid slope of α and β phases, respectively. The phase-diagram of Al-Si alloy is presented in Fig. 1.

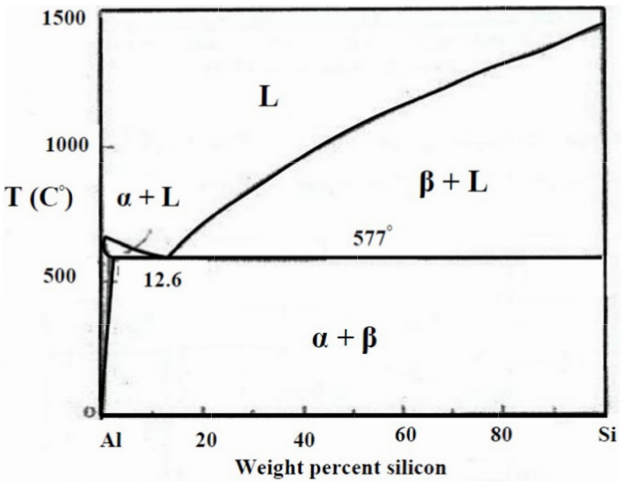

Fig. 1. Phase-diagram of Al-Si alloy [33]

TABLE 1

Materials Parameters of the Al-Si system, which are obtained from the alloy phase-diagram

Quantity	Used value
m_α	–163 k/mol
m_β	183 k/mol
C_α	1.6 mol%
C_β	99.85 mol%
C_E	12.6 mol%
D	0.5×10^{-12} m/s^2

As in the standard phase-field models [19], the interface thickness W should be larger than the average capillary length,

$\bar{d}$, to make the phase-field simulations feasible. Therefore, we choose $W/\bar{d}$ as the resolution for our model in a way that fulfills the above requirement.

We define the phase dependent relaxation time as

$$\tau\left(\vec{\phi}\right) = \bar{\tau} + \frac{\tau_\beta - \tau_\alpha}{2}\left(\frac{\phi_\beta - \phi_\alpha}{\phi_\beta + \phi_\alpha}\right) \tag{14}$$

where $\tau_i (i = \alpha, \beta)$ is the time relaxation of each individual phase and $\bar{\tau} = (\tau_\alpha + \tau_\beta)/2$. We scale lengths by W and time by $\bar{\tau}$ and get the following dimensionless parameters,

$$\tilde{\tau}\left(\vec{\phi}\right) = \frac{\tau\left(\vec{\phi}\right)}{\bar{\tau}}, \quad \tilde{D} = \frac{D\bar{\tau}}{W^2} \quad \text{and} \quad \tilde{t} = \frac{t}{\bar{\tau}} \tag{15}$$

A standard finite difference approach is used to discretize the model equations with a grid spacing $\Delta x/W = 0.8$.

The phase field and the diffusion equations, Eq. (11) and (8), are solved together by a first-order Euler Scheme with a time step of $\Delta t/\bar{\tau} = 0.0055$, which is slightly below the stability limits of both diffusion and phase-field equations, $\Delta t/\bar{\tau} = (1/4)(\Delta x/W)^2 \min[1/\tilde{D}, \tilde{\tau}_\alpha, \tilde{\tau}_\beta]$. For $\kappa_\alpha = \kappa_\beta = 0$, Eq. (13) yields, $\tilde{\tau}_\alpha/\tilde{\tau}_\beta = (|c_\beta|/|c_\alpha|)^2$.

A series of two dimensional simulations are performed in a rectangular box with symmetric boundary conditions. The simulations are started with several particles of β phases. All physical conditions are fixed, we now choose the only truly free computational parameter, the interface thickness W. As in the standard phase-field models [19], the interface thickness W should be larger than the average capillary length, $\bar{d}$, to make the phase-field simulations feasible. Therefore, we choose $W/\bar{d}$ as the resolution for our model in a way that fulfills the above requirement. Here, we set the input parameters, $W/\bar{d} = 15.085$. The coupling constant λ_c is computed by using Eq. (12).

4. Results and discussions

Now it is well established that the Al-Si eutectic can exhibit either of two morphologies an unmodified and a modified morphology. The unmodified morphology is typically coarse and flaky, while in the modified morphology the silicon spherical particles are observed [5]. We know that nucleation plays a dominant role in the modification of the Al-Si eutectic [6]. The objective of this paper is to investigate the evolution of eutectic silicon in Al-Si alloy. As stated before, We have modeled the nucleation process in Al-Si alloy by inclusion of stochastic noise terms into the phase-field equations. Here, we discuss the dominant role of fluctuations in β-Si formation and present the simulation results.

We perform the phase-field simulations for two values of C_β. According to phase-diagram of Al-Si alloy, as shown in Fig. 1, the composition of β phase in eutectic reaction is approximately

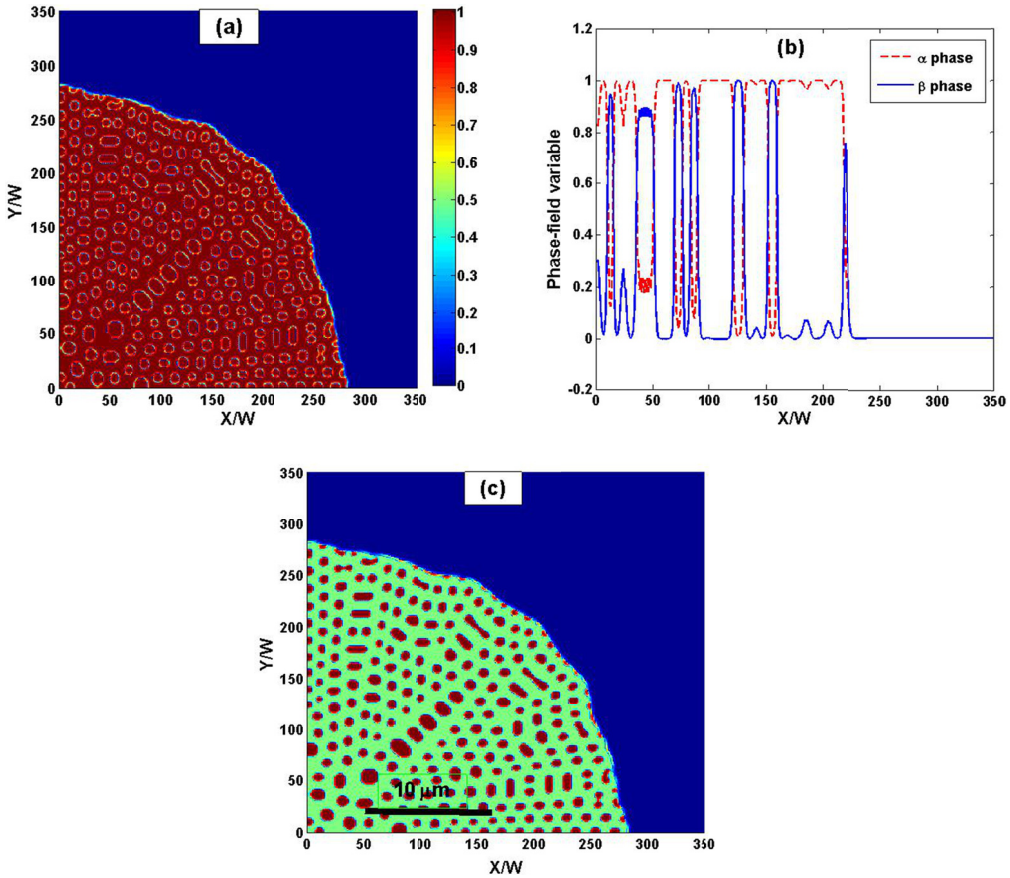

Fig. 2. Eutectic growth in Al-Si alloy with $C_\beta = 40$ mol%, the microstructure with a color map representing 1 for both solid phases and zero for the liquid (a), a plot of the α and β phase-field variables through the center of the domain (b), a plot of the dimensionless concentration through the center of the domain (c) are shown

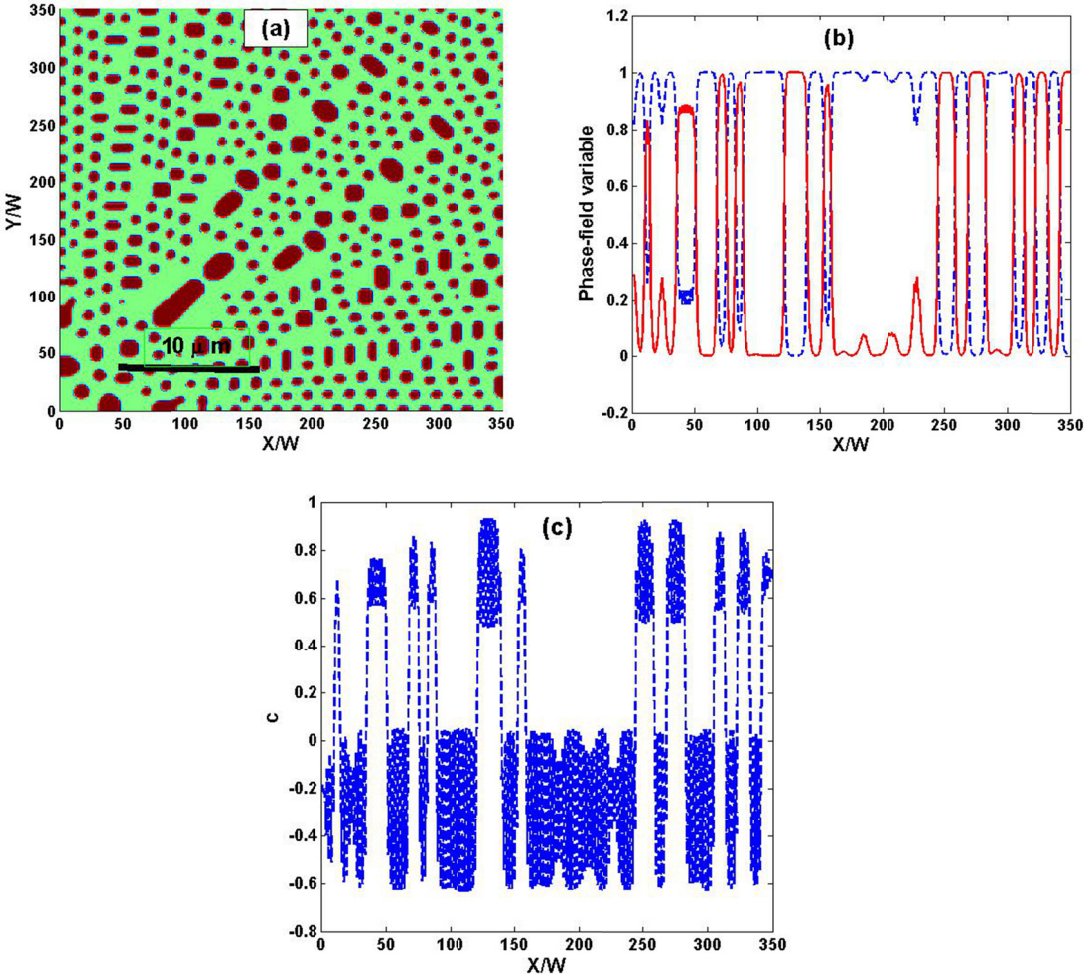

Fig. 3. Eutectic growth in Al-Si alloy with $C_\beta = 40$ mol%, the microstructure of the completely solidified domain (a), a plot of the α and β phase-field variables (b) and a plot of the dimensionless concentration (c) through the center of the domain are presented

$C_\beta = 99.85$ mol%. However, to examine the effects of β composition on spacing selection during eutectic growth in Al-Si alloy, we have performed a series of simulations with $C_\beta = 40$ mol%.

We start with a small β-Si nucleus, placed at the left-lower corner of the simulation box. The resulted microstructure, after 25000 time steps, is shown in Fig. 2(a). The color-map represents two limits; 1 for α and β solid phases and zero for the liquid. As we can see, both solid phases are presented in red color and the liquid with blue color. We use Matlab as a post-processing software. In Fig. 2(b), we have plotted α and β phase-field variables across the center of the solidification domain at $Y/W = 175$. The blue solid line is the β phase and the dashed-red line represents the α phase. We observe that sum of φ_α and φ_β in each X/W is 1. To distinguish between α and β in our graphics, we have illustrated the α phase with green color in Fig. 2(c). In the rest of this paper, except Fig. 12, we use green (light gray) color for α and red (dark) color for β phase.

Fig. 3 shows the completely solidified microstructure of Fig. 2. For this simulation, the magnitude of noise coefficients are $N_\alpha = 1.25$ and $N_\beta = 1.20$.

The fish-bone like structure in Fig. 4, is obtained by increasing the noise coefficients of previous simulation to $N_\alpha = 1.55$ and $N_\beta = 1.45$.

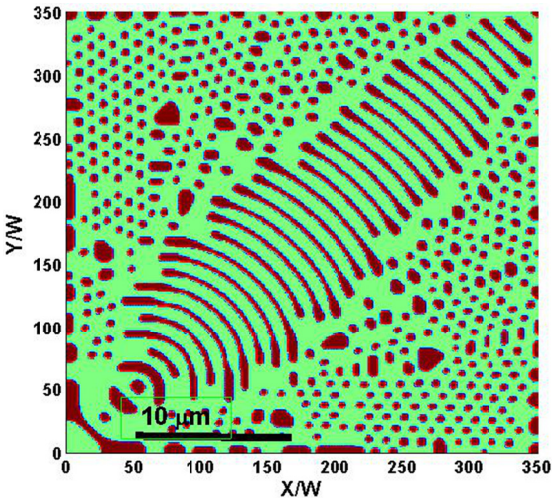

Fig. 4. Fish-bone like structure which is obtained by imposing larger amounts of fluctuations in eutectic Al-Si alloy.

The dynamics of eutectic phase transformation are given in Fig. 5, where we have performed the simulation with five nuclei of β phase. One of these particles is placed in the center of simulation box and one in each corner. All of the particles have initially the same size. The noise coefficients are $N_\alpha = 1.25$ and

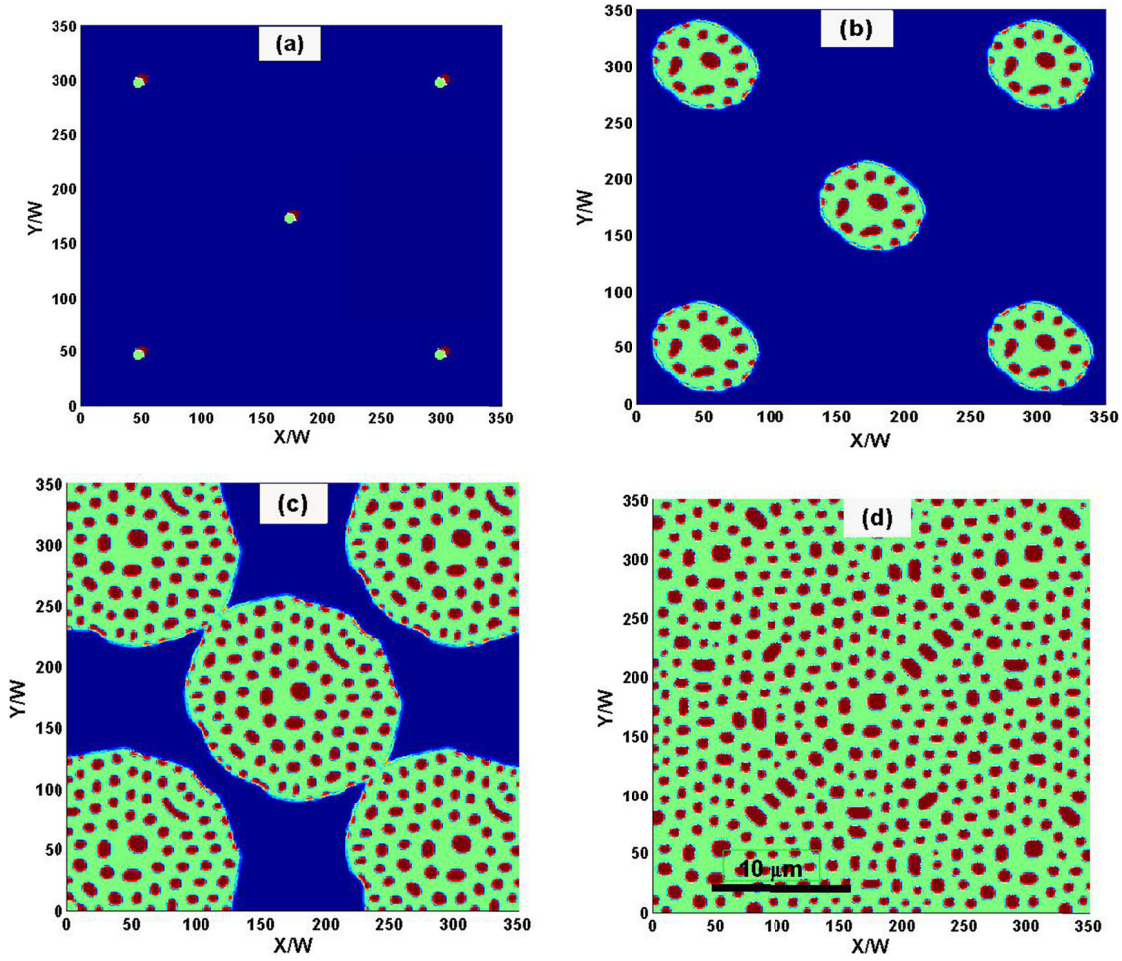

Fig. 5. Eutectic growth in Al-Si alloy with noise coefficients $N_\alpha = 1.25$ and $N_\beta = 1.20$, initial condition (a). The resulted microstructures after $t = 5000$ (b), $t = 10000$ (c) and $t = 20000$ time steps (d) are presented

$N_\beta = 1.20$. Fig. 5(a) is the initial conditions. Figs. 5(b), (c) and (d) illustrate the microstructure after 5000, 10000 and 20000 time steps, respectively. Each time step is 0.0055 s. In these pictures, the aluminum phase is represented in green and silicon phase in red and blue color shows the liquid phase. As we can see in Fig. 5(a), the α phase grows progressively and the β phase nucleates on the interface of the α phase. The volume fraction of β phase is smaller and forms as Si flakes. After that the β flakes formed, their growth stops and the α phase appears again. The nucleation and growth of β flakes take place in concentric rings around the initial nuclei. The growth of solid phases continues until the entire domain is solidified (Fig. 5(d)). At this time, the solidification process is completed and the whole liquid is solidified. The dimensions of β phase flakes are in the range of 100-500 nm.

To investigate the effects of fluctuations appearing in the solid-liquid interfaces, and to better elucidate the effects of interfacial fluctuations on growth of eutectic Si phase, the eutectic growth simulation is performed with three different noise coefficients. The results are presented in Fig. 6. The initial condition is as the previous simulation, with five grains in the simulation domain. In Fig. 6(a), (b) and (c), we have $N_\alpha = 0.95$ and $N_\beta = 0.85$, $N_\alpha = 1.25$ and $N_\beta = 1.2$ and $N_\alpha = 1.55$ and $N_\beta = 1.45$, respectively. As we can see, the β phase is nucleated in the foundation of the α phase. We have observed that the growth speed has increased with increasing of the magnitudes of fluctuation (noise coefficients) in such a way that Fig. 6(a) is obtained after 45000 time steps, Fig. 6(b) after 20000 and Fig. 6(c) after 10000 time steps. Moreover, in addition of the β-phase flakes, some needle-like and fish-bone like silicon structures are formed as the noise coefficients are increased.

The simulation results that we have presented, indicates the importance of noise inclusion in the phase-field equations to model the eutectic growth and nucleation of β-Si phase. Without noise additions, the initial grains will not grow at all and start to melt in some cases. Although the silicon flakes obtained in Fig. 6 have been observed in the start of the solidification of Al-Si melt in Bridgman experiments [1], we have used $C_\beta = 40$ mol% to obtain them. Therefore, we can not compare them with experimental results.

For more realistic results, we take the value of β composition as $C_\beta = 99.85$ mol%, according to phase-diagram of Al-Si alloy. The microstructure with one nucleus of β phase, which is placed on left-lower corner of the simulation box, is illustrated in Fig. 7. The noise coefficients are adjusted for this new system to $N_\alpha = 2.00$ and $N_\beta = 1.95$. As we expected, by increasing C_β, the volume fraction of β-Si phase is decreased and the silicon particles form in a smaller size. Fig. 7(a) is the initial condition and the eutectic microstructure is shown in Fig. 7(b), where

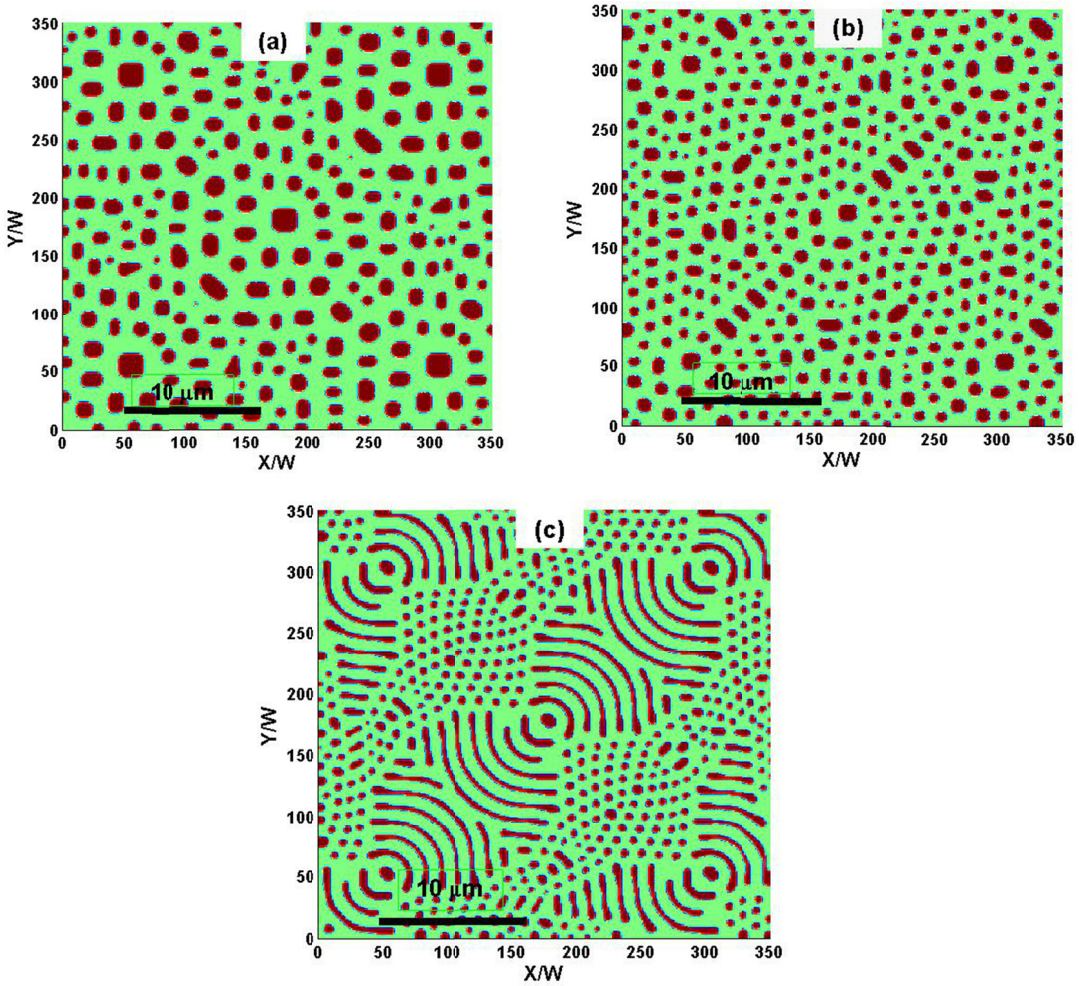

Fig. 6. Eutectic growth in Al-Si alloy with different noise coefficients. Microstructures with $N_\alpha = 0.95$ and $N_\beta = 0.85$ (a), $N_\alpha = 1.25$ and $N_\beta = 1.20$ (b), $N_\alpha = 1.55$ and $N_\beta = 1.55$ (c) are presented

β-Si particles are represented in red and the α-Al matrix in green colors. The blue color show the remaining liquid. The solidification fron is more obvious in Fig. 7(c), where we have illustrated the chemical potential, μ. The value of μ is positive on solid boundaries and negative in the liquid. The value of μ in the solidified microstructure is small compared with its value on the solidification front. Fig. 7(d) shows a plot of dimensionless concentration c across the simulation box at $Y/W = 320$. As we can see, the concentration in the β phase is $c_\beta = 0.8825$ and in the α phase is $c_\alpha = -0.1175$ and varies between these two values across the interface of α and β. c is zero in the liquid.

By imposing fluctuations with larger noise coefficients in the previous simulation, the needle-like β-Si can be obtained. For instance, the needle-like β phase in Fig. 8(a) is obtained by increasing the noise coefficients to $N_\alpha = 3.0$ and $N_\beta = 2.95$. If we consider the profile of chemical potential for this simulation, we see that needle-like silicon has a relatively low value of μ.

Next, we perform a simulation with four nuclei of β-Si. The evolution of β-Si phase is shown in Fig. 9. Fig. 9(a) is the initial condition, where we have placed the square-shape β nuclei in each corner of the simulation box. Fig. 9(b) shows the microstructure after 40000 time steps and in Fig. 9(c), the liquid is completely solidified.

The chemical potential of the microstructure of this simulation, is given in Fig. 10(a) and is plotted across the center of simulation box, $Y/W = 175$, in Fig. 10(b). The corresponding dimensionless concentration, is also presented in Fig. 11(a). A plot of c through the center of the simulation box for the completely solidifies microstructure, Fig. 11(b), shows that the value of c is positive in β phase and negative in the α phase.

In the simulations that we have performed till now, we had some nuclei of β phase. As a next step, we perform a simulation with a primary α phase. In Fig. 12(a), we have a relatively large grain of α-Al phase, which is placed on the lower-left corner of the simulation box. This is the initial condition, where the color-map shows that α is one in the red region and zero outside of it. The blue color is the liquid. The solidification microstructure is presented in Fig. 12(b). As the melt is under-cooled, first a flake of β is formed on the foundation of primary α phase anf then, the α phase nucleates on this β flake and around it. The growth of α phase continues until it takes a finger-like shape. This α finger provides a nucleation site for β-Si particles. As we can see in Fig. 12(b), the β-Si particles are formed on the foundation of α-Al matrix and are represented with yellow (light) color in this figure.

The microstructure in Fig. 9 was symmetric, since we had four initial nuclei of the same size. To break this symmetry in our

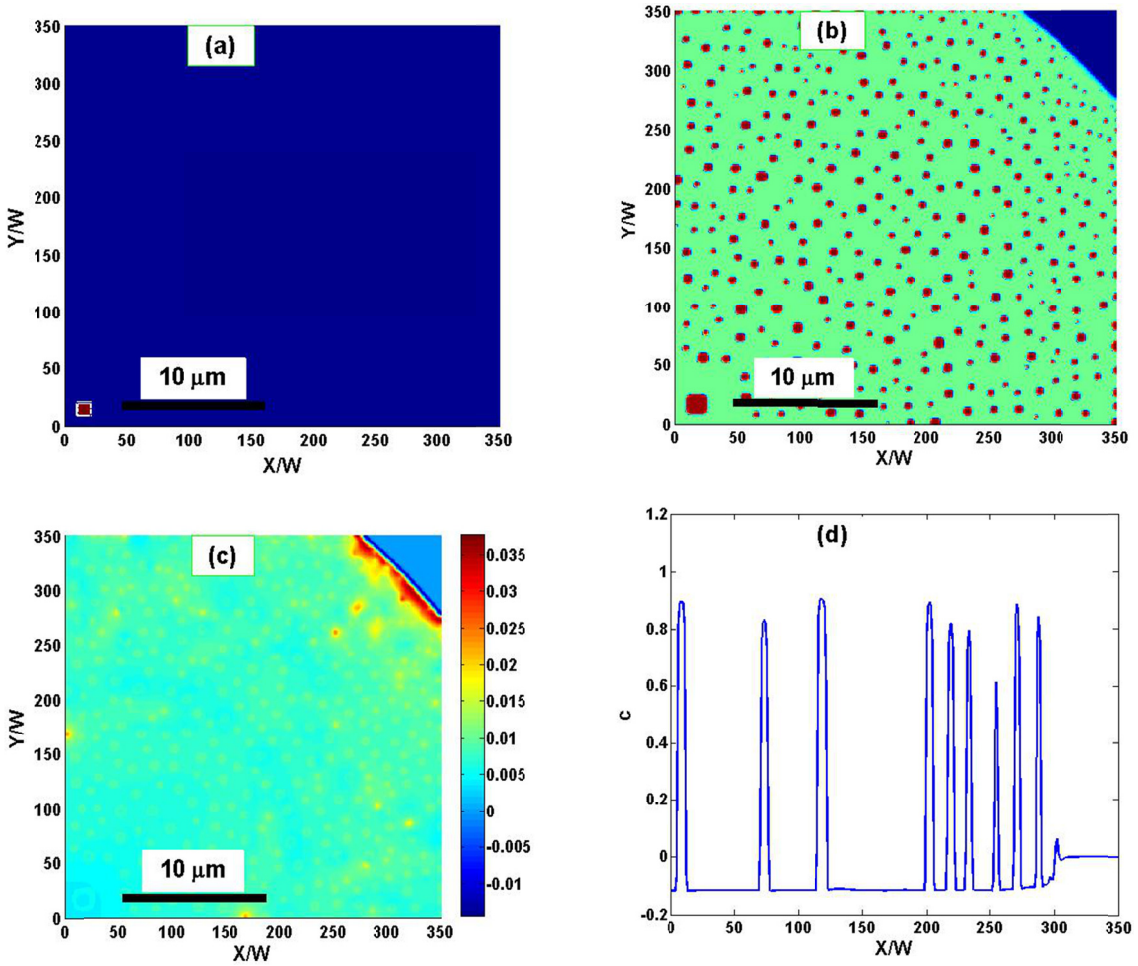

Fig. 7. Eutectic growth in Al-Si alloy with C_β = 99.85 mol%. The initial condition (a), the formation of β-Si particles with small size (b), the corresponding chemical potential (c) and a plot of chemical potential at X/W = 320 (d) are illustrated

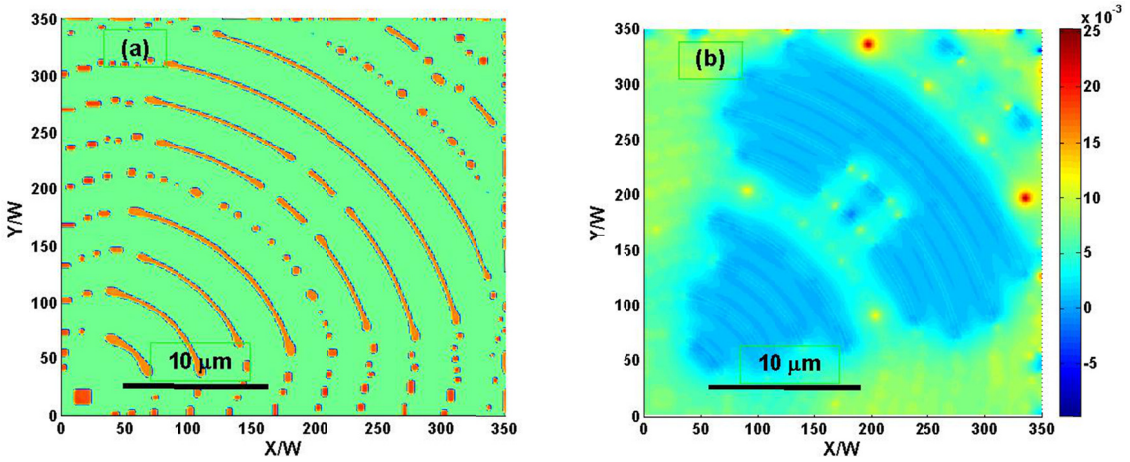

Fig. 8. Needle-like β-Si which are obtained by imposing larger amounts of fluctuations. The resulted microstructure (a) and the corresponding chemical potential (b) are shown

phase-field simulations and also to elaborate the role of primary α phase on nucleation of silicon particles in Al-Si alloy, we have performed a series of runs. In the first run, we have placed four square-shape grains, with different sizes, of β-Si on each corner of simulation domain. The resulted microstructure is shown in Fig. 13(a). As it is obvious, the α-Al phase grows on the boundary of initial β grains and the growth of α phase continues until it takes the finger-like shape. Since the initial nuclei of β phase had different sizes, the size of α fingers is not the same as well. However, the nucleation of β phase occurs on the foundation of these finger-like α-Al as before. As the solidification proceeds, the formation of β-particles continuous in radial rings, until the whole liquid is solidified. In Fig. 13(b), we have primary α phase as initial condition, with the same size and position of the previ-

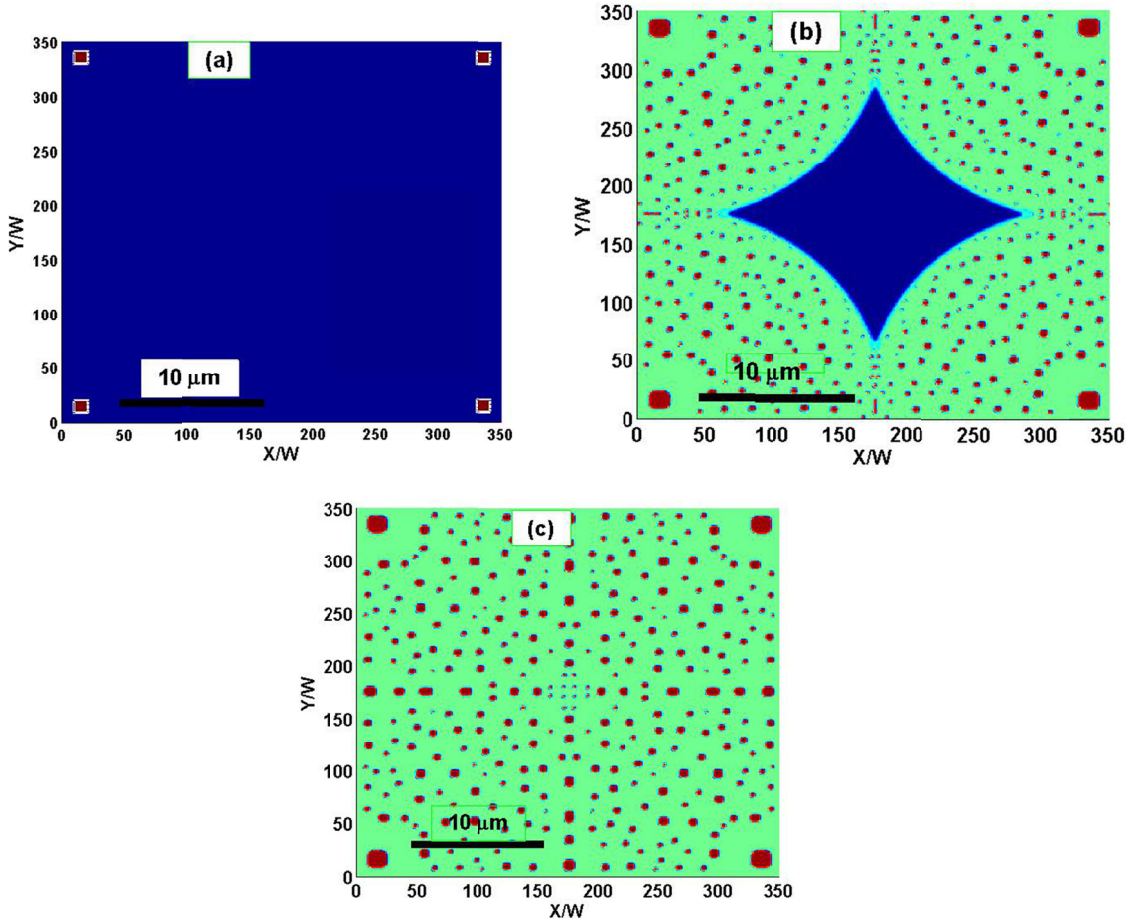

Fig. 9. Dynamics of β-Si formation with four nuclei and $C_\beta = 99.85$. The initial condition (a), the resulted microstructure after 40000 time steps (b) and the completely solidified domain (c) are presented

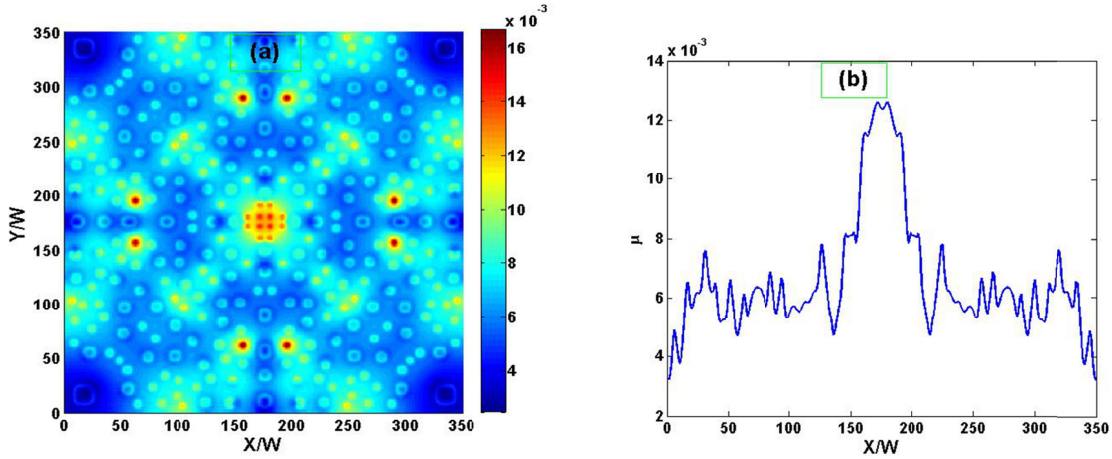

Fig. 10. Chemical potential for the completely solidified microstructure of Fig. 9(c). The chemical potential with a color map (a) and a plot of chemical potential through the center of the simulation box (b) are shown

ous run. As one can observe, the square α-Al phase grows, until it take the finger shape again and then, the β particles nucleate. Figs. 13(c) and (d) present the results of similar simulations as Figs. 13(a) and (b), respectively. The only difference is that the upper-left nucleus has a rectangular shape, with a relatively large aspect ratio. The resulted microstructure is unsymmetric, as we expected. However, the evolution of β-Si phase particles is the same as before.

We have compared our simulation results with experimental observations in Fig. 14. The finger-like α-Al phases are also observed in experimental observations of chemically modified Al-Si system, as shown in Fig. 14(b). The silicon particles appear as isolated spherical crystals, when observed at low magnification. Moreover, the eutectic in modified alloys tends to grow from the surface of a casting towards the center, see Fig. 14(a). In Fig. 14(c), in which the α phase is presented in green, one

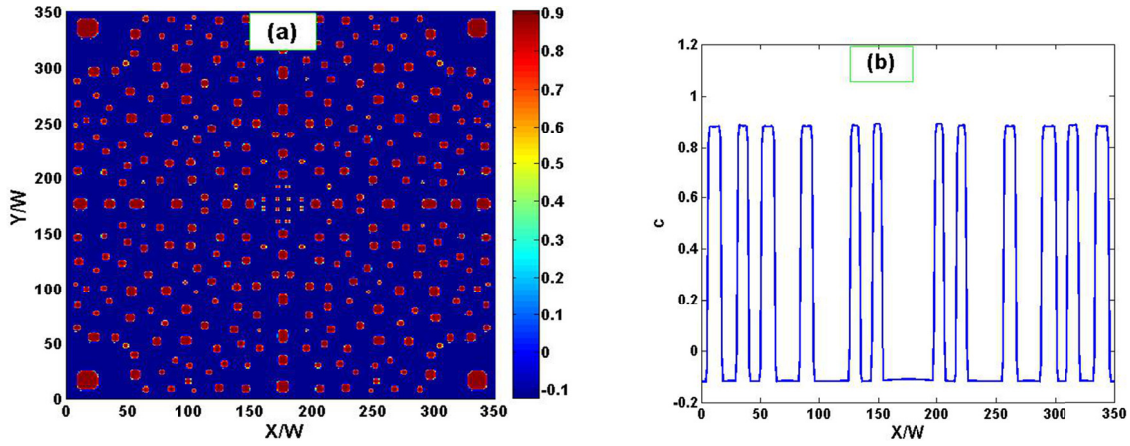

Fig. 11. Dimensionless concentration of the completely solidified microstructure of Fig. 9(c). The concentration field with a color map (a) and a plot of concentration through the center of the simulation box (b) are presented

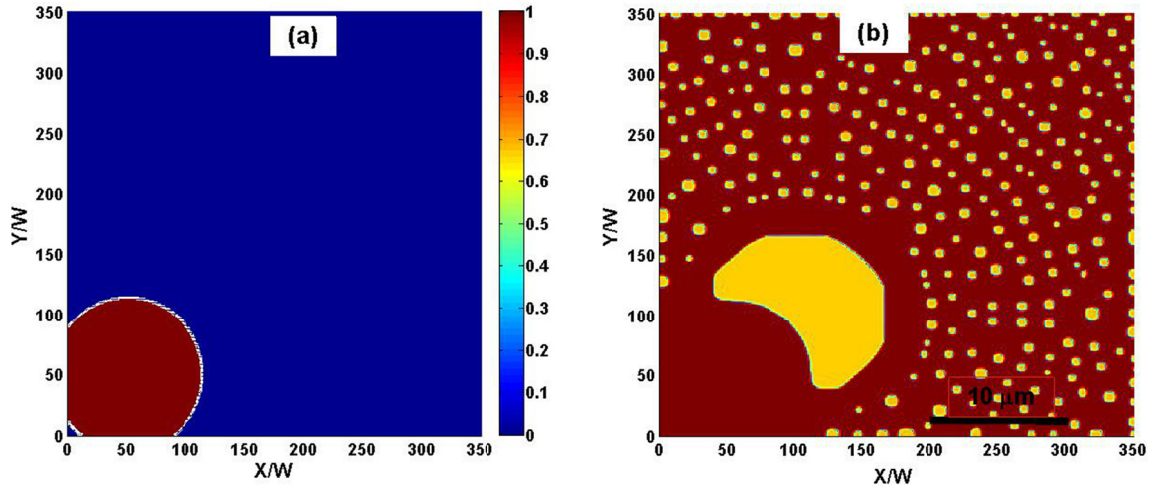

Fig. 12. Simulation with primary α phase. This figure shows the initial condition (a) and the formation of finger-like α-Al and nucleation of β-Si particles on its foundation (b)

can see that the simulated finger-like Al phase and spherical Si particles are very similar to those of experiments. This shows the capability of the presented phase-field model to simulate eutectic growth in modified Al-Si system. The fluctuations that we have added to the phase-field equations play the role of modifiers here.

The eutectic microstructure in unmodified Al-Si alloy comprises large elongated plates of silicon in the aluminum matrix. This is usually attributed to the strong anisotropy of growth of silicon [5]. Therefore, the phase-field modeling of eutectic growth in unmodified Al-Si, requires the application of an interphase boundary anisotropy to silicon phase, which is beyond the scope of this paper. This can be done as a continuation of this work. Furthermore, simulations with larger domain can also be performed to simulate more finger-like shape. This can give simulation results more similar to Fig. 14(b), which is not the case here, due to the computational costs.

5. Summary and conclusion

We have utilized a phase-field model to investigate the evolution of eutectic silicon in Al-Si alloy. The interfacial fluctuations are included into the FP phase-field model as stochastic noise terms. We have discussed the dominant role of fluctuations in β-Si formation. The effects of noise coefficients on formation of β-Si phase have been studied.

We have performed the phase-field simulations for two values of β composition. The simulation results have shown needle-like, fish-bone like and flakes of silicon phase in the case of smaller β composition, by adjusting the noise coefficients to larger values. The simulation results that we have presented, indicates the importance of noise inclusion in the phase-field equations to model the eutectic growth and nucleation of β-Si phase. Without noise additions, the initial grains started to melt, even with increasing the undercooling.

By increasing the β composition to its real value, we have obtained smaller silicon particles, as expected. We have observed that β-Si spherical particles nucleate on the foundation of primary

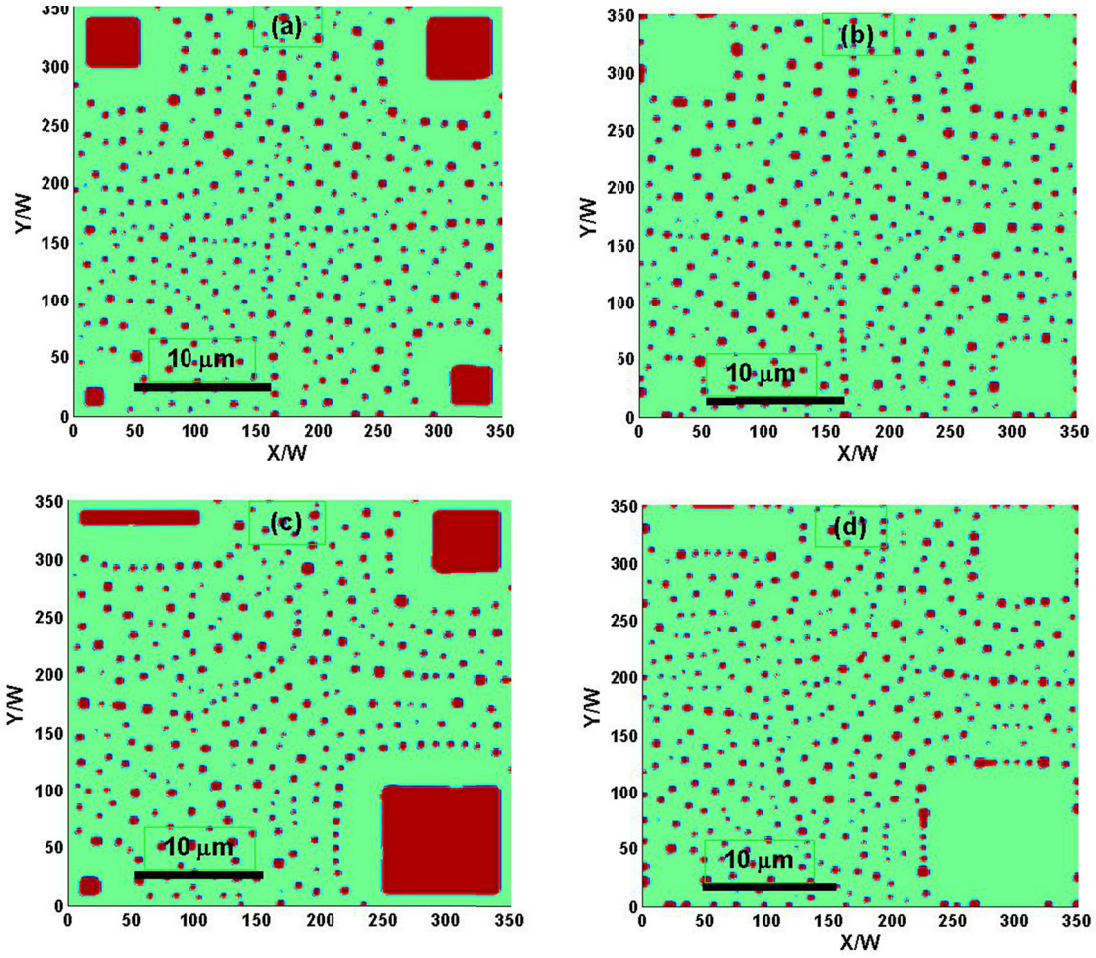

Fig. 13. Eutectic microstructure and evolution of β-Si particles on the foundation of finger-like shape α-Al. The initial condition includes four square-shape β-Si nuclei with different sizes in (a) four square-shape α-Al nuclei in (b). Unsymmetrical microstructure with primary β phase (c) and with primary α phase (d) are presented

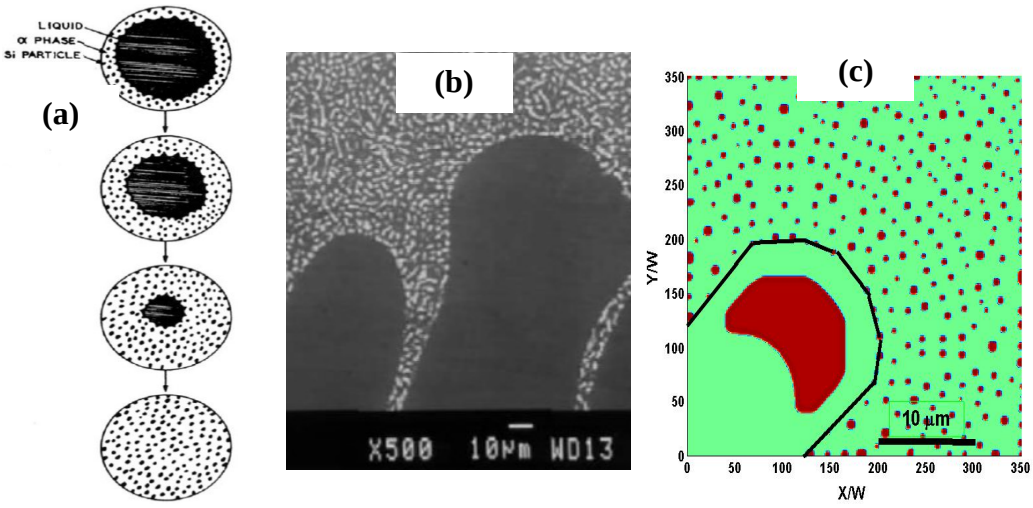

Fig. 14. Schematic diagram showing the evolution of silicon particles during solidification of a modified Al-Si eutectic [7] (a), the microstructure of a strontium modified Al-Si alloy at low magnification [5] (b) and the phase-field simulation results (c) are shown

α phase. Then the nucleation and growth of spherical Si particles continues on concentric rings through the Al matrix. We have attributed the nucleation of β-Si to inclusion of fluctuations into the phase-field equations. The role of primary α phase on nucleation of silicon particles in Al-Si alloy is elaborated by performing a series of runs with several initial nuclei of different shapes and sizes. The simulated finger-like Al phases and spherical Si particles were very similar to those of experimental eutectic growth in modified Al-Si alloy. This shows the capability of the presented phase-field model to simulate eutectic growth

in modified Al-Si system. We conclude that the fluctuations, which we have added to the phase-field equations, play the role of modifiers here.

The phase-field modeling of eutectic growth in unmodified Al-Si, requires the application of an interphase boundary anisotropy to silicon phase and can be performed as a continuation of this work. Furthermore, simulations with larger domain can also be carried out to simulate more finger-like shape Al phase, which was not the case here due to the computational costs.

REFERENCES

[1] M.W. Ullah, T. Carlberg, J. Crystal. Growth. **318**, 212-218 (2011).

[2] S.D. McDonald, N. Kazuhiro, A.K. Dahle, Acta Mater. **52**, 4273-4280 (2004).

[3] M. Gunduz, H. Kaya, E. Cadirli, A. Ozmen, Mater. Sci. Eng. A **369**, 215-229 (2004).

[4] K. Nogita, J. Drennan, A.K. Dahle, Mater. Trans. **44**, 625-628 (2003).

[5] MM. Makhlouf, H.V. Guthy, J. Light Metal. **1**, 199-218 (2001).

[6] P.B. Crosley, L.F. Mondolfo, Mod. Castings **46**, 89-100 (1966).

[7] C.B. Kim, R.W. Heine, J. Inst. Met. **92**, 367 (1963-1964).

[8] X. Bian, W. Wang, J. Qin, Mater. Sci. Forum **331**, 349-354 (2000).

[9] W. Kurz, D.J. Fisher, Fundamentals of Solidification, Trans. Tech. 1040 Publications (1998).

[10] S. Akamatsu, S. Bottin-Rousseau, G. Faivre, Philos. Mag. **86**, 3703 (2006).

[11] R. Folch, M. Plapp, Phys. Rev. E. **72**, 011602 (2005).

[12] S.D. McDonald, N. Kazuhiro, A.K. Dahle, Acta Mater. **52**, 4273-4280 (2004).

[12] K.A. Jackson, J.D. Hunt, Trans. Met. Soc. AIME **236**, 843 (1966).

[13] S. Akamatsu, M. Plapp, Current Opinion in Solid State and Mater. Sci. **20**, 46-54 (2016).

[14] S. Ghosh, A. Choudhury, M. Plapp, S. Bottin-Rousseau, G. Faivre, S. Akamatsu, Phys. Rev. E **91**, 022407 (2015).

[15] S.G. Pavlik, R.F. Sekerka, Physica A **277**, 415-431 (2000).

[16] K.R. Elder, F. Drolet, J.M. Kosterlitz, M. Grant, Phys. Rev. E **72**, 677 (1993).

[17] Z. Ebrahimi, J.L. Rezende, J. Kundin, J. Crystal. Growth. **349**, 36-42 (2012).

[18] U. Hechta, L. Granasy, T. Pusztai, B. Bottger, M. Apel, V. Witusiewicz, L. Ratke, J.D. Wilde, L. Froyen, D. Camel, B. Drevet, G. Faivre, S.G. Fries, B. Legendre, S. Rex, Mater. Sci. and Eng. R **46**, 1-49 (2004).

[19] A. Karma, W.J. Rappel, Phys. Rev. E. **57**, 4323-4349 (1998).

[20] P. Fratzl, O. Penrose, J.L. Lebowitz, J. of Stat. Phy. **95** (5), 1429-1503 (1999).

[21] K. Thornton, J. Agren, P.W. Voorhees, Acta Mater. **51**, 5675-5710 (2003).

[22] B. Echebarria, R. Folch, A. Karma, M. Plapp, Phys. Rev. E. **70**, 061604 (2004).

[23] J. Tiaden, B. Nestler, H.J. Diepers, I. Steinbach, I. Physica D. **115**, 73-86 (1998).

[24] T. Takaki, M. Ohno, T. Shimokawabec, T. Aoki, Acta Mater. **81**, 272-283 (2014).

[25] T. Takaki, M. Ohno, Y. Shibuta, S. Sakane, T. Shimokawabe, T. Aoki, J Crystal Growth **442**, 14-24 (2016).

[26] M. Asle Zaeem, H. Yin, S.D. Felicelli, Appl. Math. Modell. **37**, 3495-3503 (2013).

[27] P.C. Bolladaa, C.E. Goodyera, P.K. Jimacka, A.M. Mullisa, F.W. Yang, J Comput. Phys. **287**, 130-150 (2015).

[28] R.S. Qin, H.K Bhadeshia, Mater. Sci. and Technol. **26**, 803-811 (2010).

[29] A.A. Wheeler, W.J. Boettinger, G.B. Macfadden, Phys. Rev. A. **45**, 7424 (1992).

[30] Y. Wang, D. Banerjee,C.C. Su, A.G. Khachaturyan, Acta Mater. **46**, 2983-3001 (1998).

[31] Z. Ebrahimi, J.L. Rezende, H. Emmerich, Metall. Mater. Trans. A **44**, 1925-1936 (2013).

[32] K. Kassner, C. Misbah, Phys. Rev. A **44**, 6513-6533 (1991).

[33] J.L.Murray, A.J.McAlister, Bull. Alloy Phase Diagrams **5**, 74-84 (1984).

[34] D. Cao, Y. Liu, X. Su, J. Wangb, H. Tu, J. Huang, J. Alloys Compd. **551**, 155-163 (2013).